

Article

Hydro-Volcanism in the Longgang Volcanic Field, Northeast China: Insights from Topography, Stratigraphy, Granulometry and Microtexture of Xidadianzi Maar Volcano

Bo Zhao ^{1,2,*}, Debing Xu ³, Zhida Bai ³ and Zhengquan Chen ^{1,2}

¹ National Observation and Research Station of Jilin Changbaishan Volcano, Institute of Geology, China Earthquake Administration, Beijing 100017, China

² Key Laboratory of Seismic and Volcanic Hazards, China Earthquake Administration, Beijing 100017, China

³ School of Earth Sciences and Resources, China University of Geosciences, Beijing 100190, China

* Correspondence: zhaobo@ies.ac.cn

Abstract: Hydro-volcanism in the Longgang volcanic field (LVF) of Northeast China has produced a dozen maars with features of complex sequences. To better understand the formation mechanism of maar volcanos in the LVF, this study focuses on the Xidadianzi (XDDZ) maar volcano, located in the Jinchuan valley of the LVF. Based on detailed stratigraphy analysis, ¹⁴C geochronology, grain-size distribution, and scanning electron microscopy (SEM) analysis, the eruptive sequence of the XDDZ volcano, including the South Crater and the North Crater, was constructed. The whole sequence was formed after four eruptive phases, including a wet phreatomagmatic eruption, an explosive magmatic eruption, a dry and hot phreatomagmatic eruption, and a small explosive magmatic eruption. ¹⁴C geochronology indicates that the formation age of XDDZ is 15,900 ± 70 years, BP. Topographic and stratigraphic characteristics show that the landforms of two craters were damaged and buried because of the destruction of lava flows and agricultural modification. The NE-trending fissure in the hard rock area is thought to participate in the formation of the XDDZ maar volcano.

Keywords: Longgang volcanic field; hydro-volcanism; maar volcano; fissure system



Citation: Zhao, B.; Xu, D.; Bai, Z.; Chen, Z. Hydro-Volcanism in the Longgang Volcanic Field, Northeast China: Insights from Topography, Stratigraphy, Granulometry and Microtexture of Xidadianzi Maar Volcano. *Minerals* **2022**, *12*, 1113. <https://doi.org/10.3390/min12091113>

Academic Editors: Sergei Khromykh and Andrei Tsygankov

Received: 28 June 2022

Accepted: 26 August 2022

Published: 31 August 2022

Publisher's Note: MDPI stays neutral with regard to jurisdictional claims in published maps and institutional affiliations.



Copyright: © 2022 by the authors. Licensee MDPI, Basel, Switzerland. This article is an open access article distributed under the terms and conditions of the Creative Commons Attribution (CC BY) license (<https://creativecommons.org/licenses/by/4.0/>).

1. Introduction

Maar-diatreme volcanoes, which occur all over the world, are the second-most common type of volcano [1–4]. Typical maar volcanoes are the products of individual phreatomagmatic explosions, which begin at a certain depth below the surface and gradually deepen when the water runs out [1,2]. Many studies have shown that some maar volcanoes have the feature of multiple eruptions [5–16]. Multiple eruptions consistently produce complex stratigraphic sequences. In recent years, Valentine et al., 2017 proposed a new model to explain maar-diatreme volcanoes [17]. Phreatomagmatic explosions may occur in the shallower area, led by the diatreme shifting in the vertical and lateral directions.

Northeast China presents many monogenetic intraplate volcanic fields with many products of phreatomagmatic eruptions, such as Longgang, Jingpohu, Wudalianchi, Aershan, and Chaihe (Figure 1a). Among these volcanic fields, the Longgang volcanic field (LVF) possess the largest number of maar volcanoes.

Since the 1980s, a large number of studies on volcanic geology, chronology petrology, and geochemistry have been carried out in the LVF [5,15,16,18–40]. Some researchers have focused on the deposits of maar lakes in the LVF for explaining paleoclimate change in Northeast Asia [19,41–47]. Over the last 20,000 years, at least four eruptive events have occurred in the LVF, including two Holocene eruptions [5,15,18,19,48]. The discovery of several tephra layers in the maar lake deposits shows there were probably more eruptions in the last 15,000 years [18]. The analyses of seismic and levelling data indicate that the activity of the LVF is increasing [49,50]. Pang et al., 2016 proposed that there was a low-velocity layer in the middle crust under the Jinlongdingzi volcano [51], which erupted in

1540 ± 40 a. BP. Above all, the previous works show that the LVF is an active volcanic field and has a potential eruptive risk.

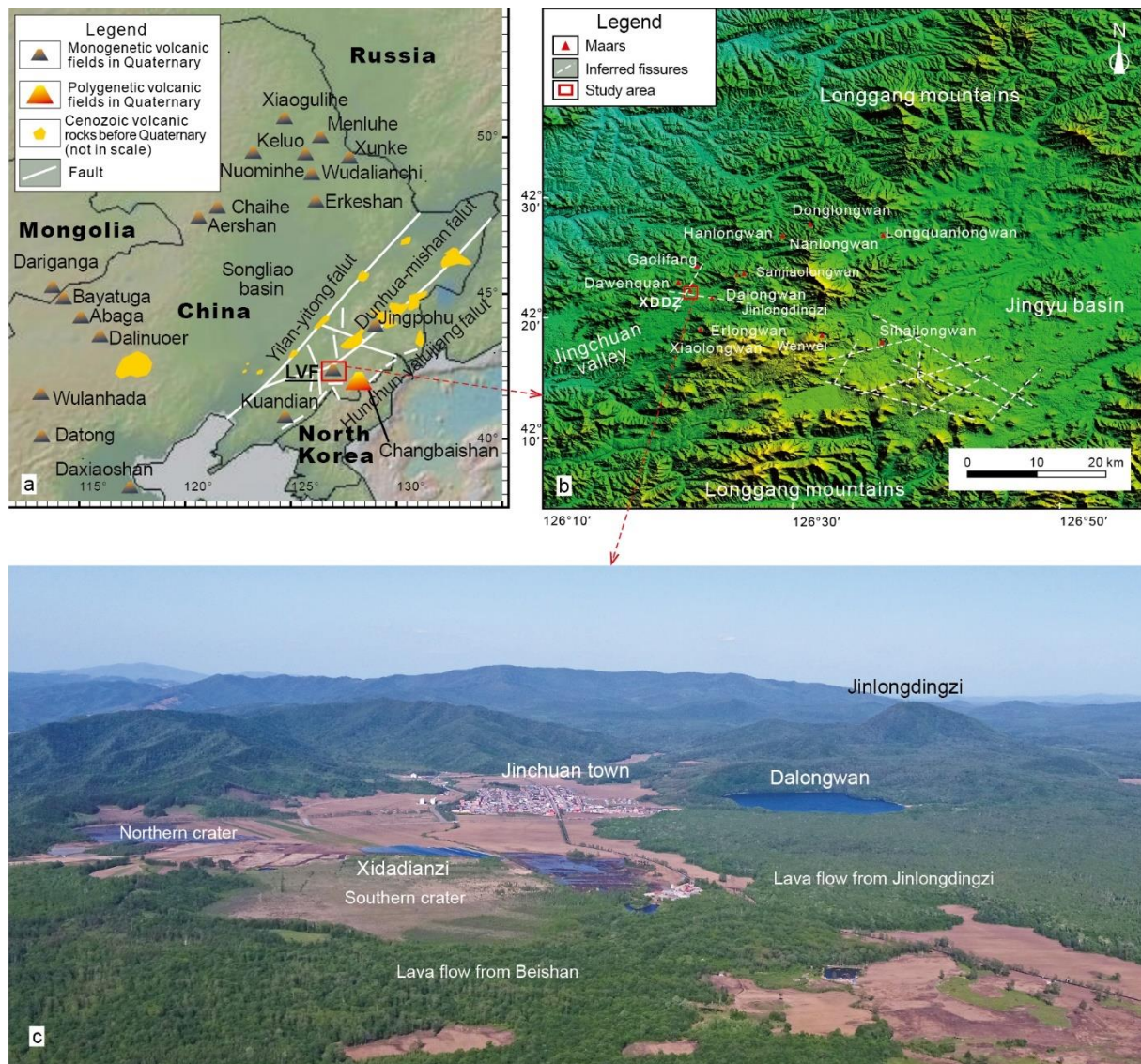


Figure 1. (a) Distribution of Quaternary volcanic fields in NE China and the location of the LVF, modified after Zhao, 2021 [15]; (b) distribution of maars in the LVF (the Digital Elevation Model map from Alos, JAXA); (c) aerial picture in the west of Jinchuan valley.

The LVF covers an area of 1550 km², producing more than 100 volcanoes, including scoria cones and maars volcanoes. Hydro-volcanism is a prominent feature of the LVF. It has produced a large number of base-surge deposits and at least 15 maar volcanoes with lakes or swamps. There are 9 Longwans (dragon bays) in the LVF, including Dalongwan, Erlongwan, Sanjiaolongwan, Sihailongwan, Donglongwan, Nanlongwan, Longquanlongwan, Xiaolongwan and Hanlongwan. All of the Longwans have been interpreted as maar volcanoes [20,52]. The K-Ar dating results show that Dalongwan, Sanjiaolongwan, Longquanlongwan, and Donglongwan were formed in the Middle-Late Pleistocene [18]. Xidadianzi (XDDZ, a big swamp in the west) was the biggest dry maar volcano in the LVF [20]. According to the ¹⁴C age, Zhao et al., 2021 proposed that XDDZ was formed in 15,590 ± 50 a. BP [15]. Base-surge deposits from Dawenquan, Wengquan, Wengwei and Gaolifang also have been found in volcanological studies [5,31]. Multiple explosions with more than two craters, are an important feature of maar volcanoes in the

LVF [5,15,16,20,31,34]. The source of volcanoes' base-surge deposits are not clear because of complex eruptive sequences in a high dense volcano distribution area. Therefore, relatively few systematic stratigraphic studies have been conducted on the base-surge deposits of maar volcanoes, and the formation process of these maar volcanoes is still unknown. In recent years, agricultural modification has exposed some sections of XDDZ maar, offering a good opportunity to carry out systematic geological investigation.

To better understand the dynamic processes of the base-surge of maar volcanoes in the LVF, we investigate the XDDZ volcano using its topography, stratigraphy, granulometry, micro texture, and major elements, so as to establish the formation model of maar volcanoes in the LVF.

2. Geologic Setting

The LVF is in the middle of the Longgang Mountains, Jilin province, NE China, with an area of 1550 km². It is a monogenetic volcanic field characterized by intra-plate volcanism [30]. The Pacific slab is believed to have played a significant role in the intra-plate volcanism of the LVF [52–55].

The country rocks of pre-Cenozoic age in the LVF include Archean supracrustal metamorphic rocks, a few Cambrian and Ordovician strata of carbonate, and clastic rocks [56]. Most of the surroundings are hard rocks, with the characteristics of high density, low porosity, and low permeability.

The tectonic setting of the LVF is along the Dunhua–Mishan fault, the Hunchun–Yalujiang fault, and several small faults (Figure 1a), at the margin of the North China craton [31,53]. The distribution of volcanoes in the LVF is mainly controlled by NE-, NW- and WE-trending faults [53]. Xu et al., 2005 inferred that the fissure system might offer the channels of interaction between water and magma [31].

The eruptions of the LVF started in the Neogene and ended in the Holocene. It can be mainly divided into two parts, Jingyu basin and Jinchuan valley, as well as several small valleys (Figure 1b). For 20,000 years, most of the eruptions have occurred in the Jinchuan valley.

3. Materials and Methods

3.1. Topographic Analysis

The purpose of the topographic analysis was to study the characteristics of the XDDZ maar volcano. The topography of maar has a close relationship between the crater distribution and the local fissure system. We applied structure-from-motion-multiview stereo (SFM-MVS) techniques on unmanned aerial system imagery to build high-resolution topographic models. The SFM-MVS process starts by acquiring photographs of the object of interest with sufficient overlap from multiple positions and/or angles. The topographic data, including 49 images and 67,160 points, were obtained from Dajiang inspire 2 with Resolution 40 cm per pix. The Agisoft photoscan (Agisoft LLC, St. Petersburg, Russia) and Global mapper 21.0 (Blue Marble Geographics, Hallowell, ME, USA) were used to build the XDDZ maar digital elevation model (DEM). Three survey lines with the trends of NE, NS, and EW, were built in the DEM map. This analysis was used to identify the crater distribution and geometric parameters (diameter, area, and height) of the XDDZ maar volcano.

3.2. Field Geological Investigation

A geological field investigation was conducted to collect samples and describe the strata of the XDDZ maar volcano in the LVF. Geological surveys, with a total of 20 working points and cross profiles, were performed around the XDDZ maar volcano. Well-exposed outcrops were selected for mapping and sampling.

3.3. ^{14}C Dating

A carbonized tree in the base-surge and scoria layers was found in the field, and we got a sample from the surface of the carbonized tree. The sample was sent to the Beta laboratory in Miami, FL, USA. All work was done at Beta in an NEC accelerator mass spectrometer and with Thermo isotope ratio mass spectrometers. The age was calculated using the Libby half-life (5568 years), corrected for total isotopic fraction, and was used for calendar calibration where applicable.

3.4. Granulometry

The grain size of samples in the field was measured and analyzed. The grain diameters were from 0.0625 (4 phi) to 64 mm (−6 phi) with 1 phi(φ) intervals (where $\varphi = -\log_2 d$). The weight of the samples was between 500 to 1000 g, and a vibrating screen was used. The median diameter (Md_φ) indicates the central size tendency. Graphical standard deviation (σ_φ) is a measure of sorting [57]. Skewness (α_φ) is used to describe the graphic asymmetry. The formulae are $Md_\varphi = \varphi_{50}$; $\sigma_\varphi = (\varphi_{84} - \varphi_{16})/2$; and $\alpha_\varphi = (\varphi_{84} + \varphi_{16} - 2\varphi_{50})/2\sigma_\varphi$. φ_{50} , φ_{84} , and φ_{16} represent a grain size of 50%, 84%, and 16% cumulative weight percentage, respectively.

In the field, we measure the size of the maximum juvenile and lithic clasts with a tape measure. A total of 48 grain-size analyses were performed. Samples were sieved using a set of sieves with mesh sizes in the Key Laboratory of the Seismic and Volcanic Hazard, Institute of Geology, Chinese Earthquake Administration. Based on the grain-size data, histograms were plotted, and the statistical parameters of Md_φ , σ_φ , and α_φ were obtained. This method was used to compare the grain sizes of the samples from different stratigraphic layers.

3.5. Microanalysis

The surface characteristics of the base-surge deposits and scoria fall were carried out at the microscopic level using microanalysis. This study used a scanning electron microscope (SEM) to examine the microstructure of the base-surge deposits, and the surface characteristics of the small-particle scoria from different layers.

We collected a base-surge sample in a hard layer of the Lg-11. In order to protect the original structures, the sample was first cemented with epoxy resin, and then it was made into a thin section. We choose the scoria from the base surge deposits, yellow scoria close to the carbonized tree and black scoria fall in Lg-11. The grain sizes of scoriae are between 0.0625–0.25 mm. We used an auto carbon coater (JEC-560, JEOL Ltd., Tokyo, Japan) to spray carbon on the surface of the thin section and scoria samples.

Samples were analysed using a JEOL JSM-6701F (JEOL Ltd., Tokyo, Japan) scanning electron microscope (SEM) in the Key Laboratory of Seismic and Volcanic Hazard, Institute of Geology, Chinese Earthquake Administration. The operation parameters included a 15 kV acceleration voltage, 10 μA electron current, and a magnification ranging from $\times 100$ to $\times 2000$. The SEM was operated between 15–25 $^\circ\text{C}$.

3.6. Major-Element Analysis

A major-element analysis was applied to understand the geochemical composition of the scoria in the XDDZ maar. Black scoriae were selected. They were tested in the laboratory of the Institute of Regional Geology and Mineral Resource Investigation in Heibe Province, China. The equipment consisted of an Axiosmax X-ray fluorescence spectrometer, a P124S Electronic analytical balance, and Burettes. The ambient temperature of the laboratory was between 18 and 27 $^\circ\text{C}$. The geochemical analysis was based on the LOI-free contents.

4. Results

4.1. Topographic Characteristics of XDDZ Maar

Topography is an important feature used to describe volcano landforms. The XDDZ maar is located in the west of Jinchuan valley (Figure 1c). In this paper, we built a high

resolution (40 cm/px) DEM of the XDDZ maar volcano (Figure 2a). Three topographic sections have been built for the analysis of XDDZ landforms (Figure 2b–d). It is composite in form, including a northern and a southern crater, with an area of 1.17 km² (Table 1).

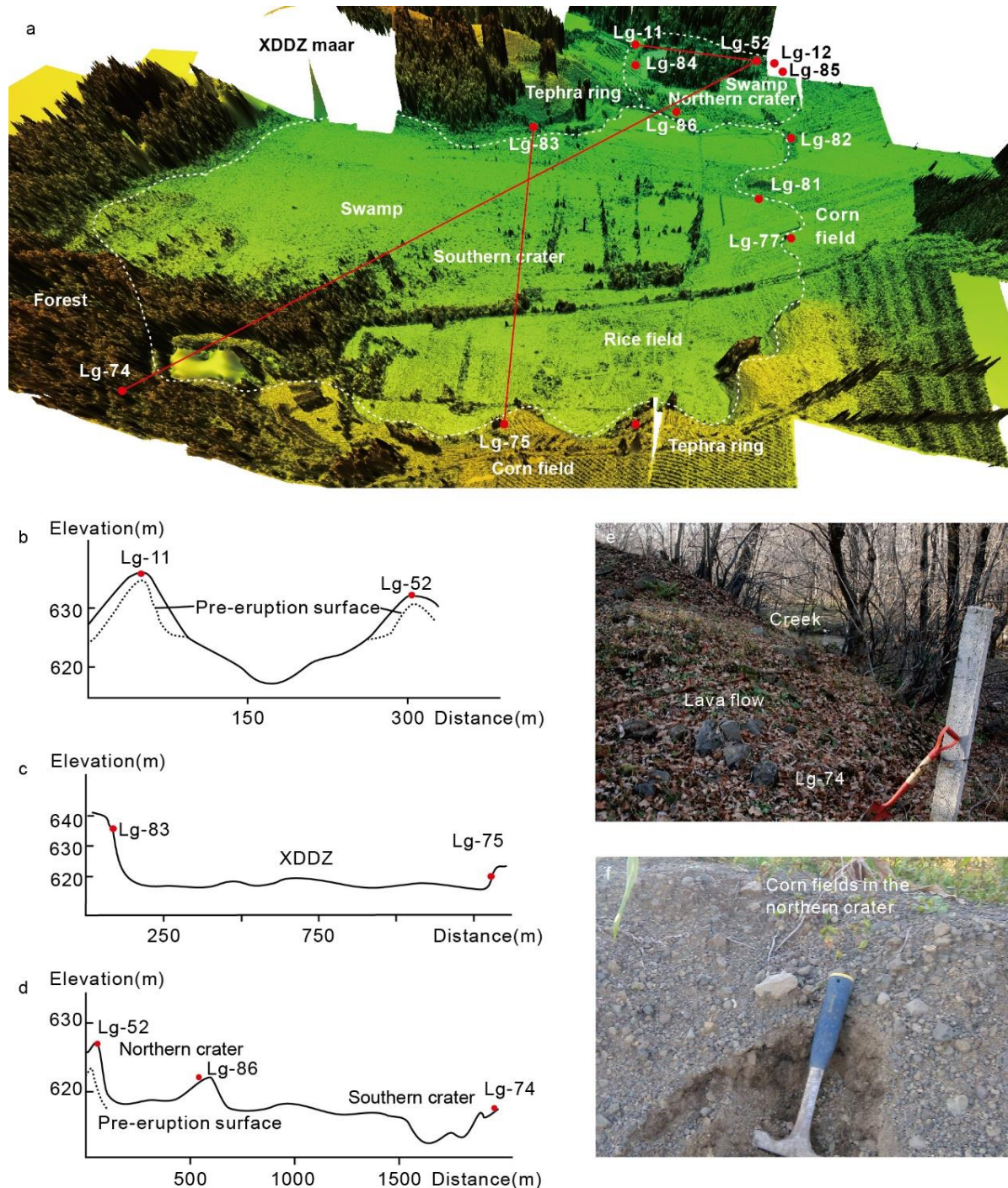


Figure 2. (a) DEM of XDDZ maar; (b) topographic section from Lg-11 to Lg-52; (c) topographic section from Lg-83 to Lg-75; (d) topographic section from Lg-52 to 74; (e) lava flow of section Lg-74, in the south of XDDZ; (f) corn field in the northern crater.

The volcanic topography of the southern crater was partly damaged. The shape of southern crater is also irregular. In the north, there is a small irregular protrusion (Figure 2a). The maximum diameter of the southern crater is 1400 m. It is higher in the northwest and lower in the south, with elevations mainly ranging between 615 m and 621 m inside the

south crater. Swamp and rice fields are distributed inside the crater, and corn fields are outside the crater. The Jinlongdingzi lava flow from the east destroyed the southeastern tephra ring, and the Beishan lava flow from west destroyed the southwestern tephra ring (Figure 1e). A creek crosses the boundary of the lava flows.

Table 1. Parameters of topography in the XDDZ maar volcano.

Crater Name	Swamp Elevation	Diameter (km)	Area of Crater (km ²)	Area of Swamp (km ²)	Height of Tephra Ring (m)
Southern crater	615~621	1.1~1.3	1.08	0.73	30
Northern crater	619~620	0.3	0.09	0.02	10

The landform of the northern crater was severely damaged. Only the northern part of the tephra ring is well preserved. The pre-eruption surface can be observed in some sections, which expose the hard country rocks. The maximum diameter of the northern crater is probably 300 m. In the center of the crater is a small swamp. The rest has been modified to rice fields. It is flat inside the crater, with elevations mainly ranging between 619 m and 620 m. Between the two craters, there is a small corn field (Figure 2f). The maximum elevation of the corn field is 625 m.

In summary, the topography of the XDDZ maar volcano is not intact. The modern topography of XDDZ maar can be divided into six main zones: residual tephra ring, swamps, rice fields, corn fields, and lava flows, as well as a creek (Figure 2a,e,f).

4.2. Stratigraphic Characteristics of XDDZ Maar

4.2.1. Proximal Stratigraphic Characteristics of XDDZ's Southern Crater

Lg-74's profile (42°29'02" N, 126°21'32.18" E) is the Jinlongdingzi lava flow front, to the south of the southern crater (Figure 2e). A creek flows along the edge of the lava flows. The southern part of tephra ring was destroyed by lava flows.

In the southeast of the southern crater, Lg-75's profile (42°20'30.79" N, 126°22'6.68" E) preserves 8 m thick strata (Figure 3a). Lg-75's profile can be subdivided into two major layers from bottom to top. Layer 1 is composed of 4 m thick base-surge deposits consisting of two parts. The bottom part is a grey massive lapilli bed, supported by the ash matrix, with a thickness of 3.4 m. It has no obvious bedding. Ballistic fragments occur around impact sags. Most of the fragments are country rocks. It has fewer juvenile fragments. The upper part is a 0.6 m ash layer. Planar beds are common in this part (Figure 3d,e). Layer 2 is composed of 4 m dark scoria-fall deposits. A bomb-rich layer is in the middle of Layer 2 (Figure 3b). The maximum diameter of these volcanic bombs can reach 1 m. Cauliflower bombs and bread-crust bombs have also been discovered (Figure 3b,c). Between L1 and L2, there is a thin baked layer.

In the northwest of the southern crater, the Lg-77 profile (42°20'43.19" N, 126°22'22.84" E) exposes a yellow scoria layer, with the thickness of 3 m (Figure 3f). Volcanic bombs occur in this layer. The maximum diameter of these bombs is 0.8 m.

In the north of the southern crater, the Lg-82 profile (42°21'6.65" N, 126°22'13.57" E) is a 3 m yellow scoria layer. It extends 140 m long, without volcanic bombs (Figure 3g).

4.2.2. Proximal Stratigraphic Characteristics of XDDZ Northern Crater

The residual tephra ring only occurs in the north, including the profiles of Lg-11, Lg-12, Lg-52, Lg-84, and Lg-85 (Figure 4). We can get information about the primitive tephra ring in the northern crater from these residual strata. The Lg-11 profile (42°21'21.53" N, 126°22'5.61" E) is a typical section in the northern crater, consisting of three layers from bottom to top with a thickness of 4.3 m (Figure 5a).

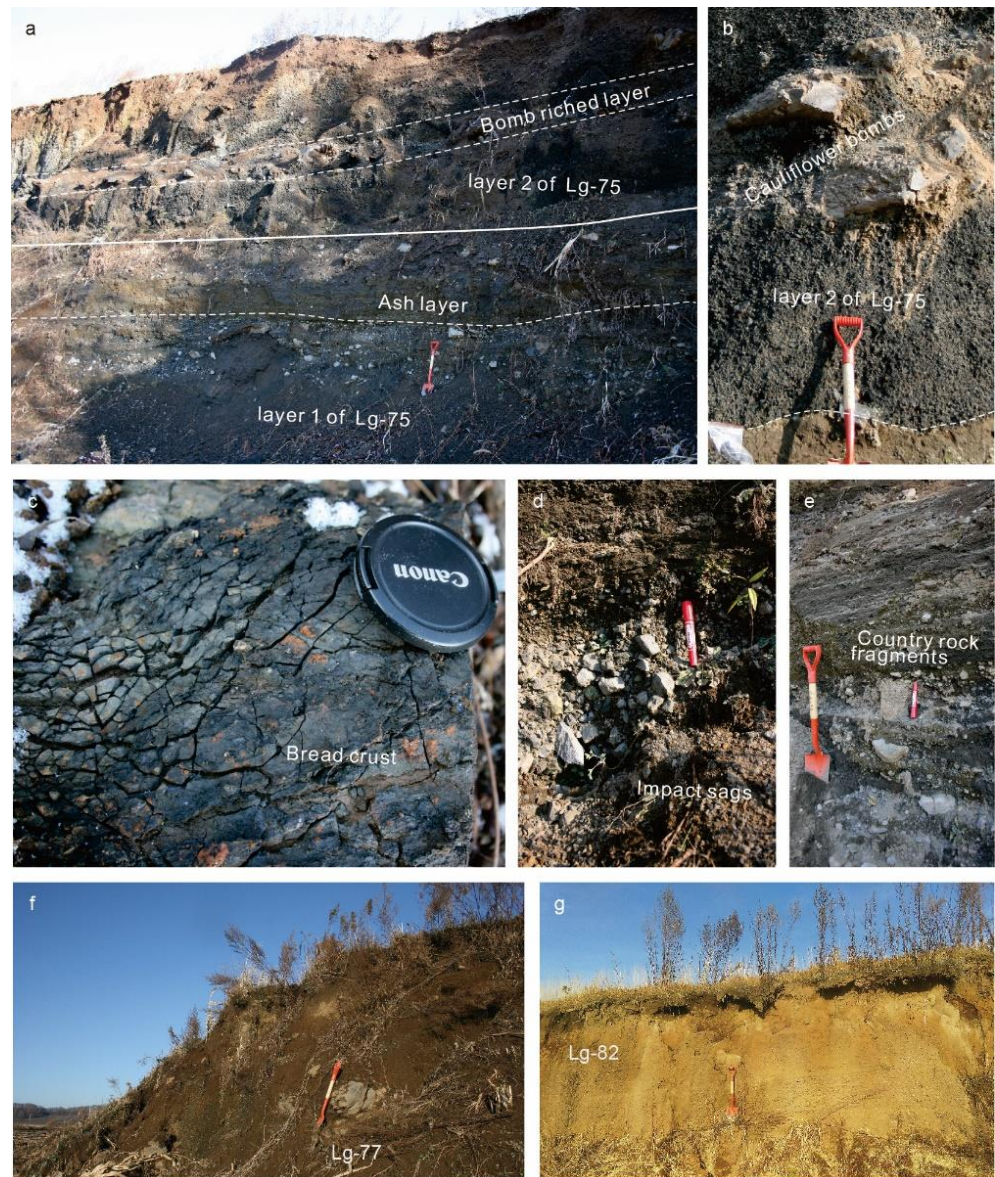


Figure 3. The proximal strata of the southern crater: (a) overview of Lg-75; (b) cauliflower bombs in the bomb-rich layer of Lg-75; (c) bread crust bomb of Lg-75; (d) impact sags of Lg-75; (e) planar layers and lithic-rich layers of Lg-75; (f) overview of section Lg-77; (g) overview of section Lg-82. Lens cap: 6 cm; red marking pen: 15 cm; shovel: 80 cm.

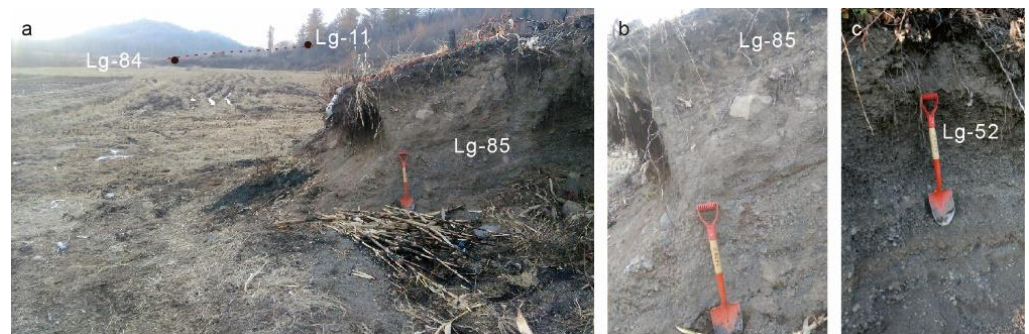


Figure 4. Cont.



Figure 4. The proximal strata of the northern crater: (a) overview of the residual tephra ring from Lg-85 to Lg-84 (from east to west); (b) explosive breccia layers in the upper part of Lg-85; (c) a scoria layer in the upper part of Lg-52; (d) a collapsed gap in Lg-84; (e) scoria and base surge layers in the Lg-84; (f) a carbonized tree in Lg-12.

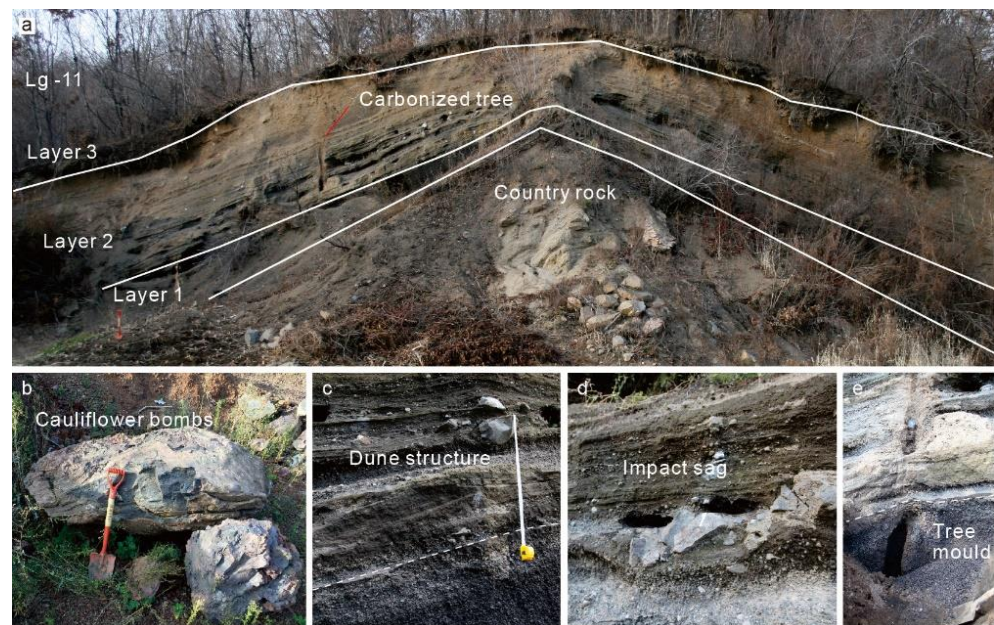


Figure 5. The proximal stratum of Lg-11 of the northern crater: (a) overview of section Lg-11; (b) cauliflower bomb; (c) dune structure; (d) impact sags with country rock fragments; (e) a tree mould in layer 1 and layer 2.

In the bottom of Lg-11, layer 1 is a dark scoria-fall layer with a thickness of 1 m. The scoria is angular and vesicular. There are no volcanic bombs in the scoria layer. It contains abundant carbonized wood. The country rocks are exposed under the layer 1 (Figure 5a).

In the middle of Lg-11, layer 2 is a 3 m thick base-surge layer. It is formed by thin layers and thick layers, which make many rhythmic layers. The thin layers are supported by the ash matrix, developing cross bedding, dune bedding and a sag structure, with a thickness of 3–20 cm. The thick layers are of clast-supported structure, with a thickness 10–30 cm. These clasts consist of country rock fragments, ballistic bombs, lherzolite fragments, and more scoria (Figure 5b–d). A carbonized tree through layer 1 and layer 2, has been discovered. It forms a carbonized tree mould (Figure 5a,e). The color of scoria close to the skin of the carbonized tree is yellow, which is different from the black scoria. Another carbonized tree has been discovered in the base surge deposits in Lg-12 (Figure 4f), 250 m away from Lg-11.

At the bottom of Lg-11, layer 3 is a yellow scoria layer with a thickness of 30 cm. There are a lot of plant roots in this layer.

4.2.3. Medial Stratigraphic Characteristics from the Northern Crater

Lg-94 ($42^{\circ}21'30.21''$ N, $126^{\circ}22'20.12''$ E) is located on the top of a hill in the northeast of XDDZ, 440 m away from the center of the XDDZ northern crater (Figure 6a,b). It has the same stratigraphic sequence as Lg-11, consisting of 3 layers with a thickness of 1.8 m. At the bottom of Lg-94, layer 1 is a 40 cm dark scoria-fall layer. In the middle, layer 2 is composed of 1.3 m grey and yellow base-surge deposits, with cross bedding. At the top, it has a 10 cm scoria layer.

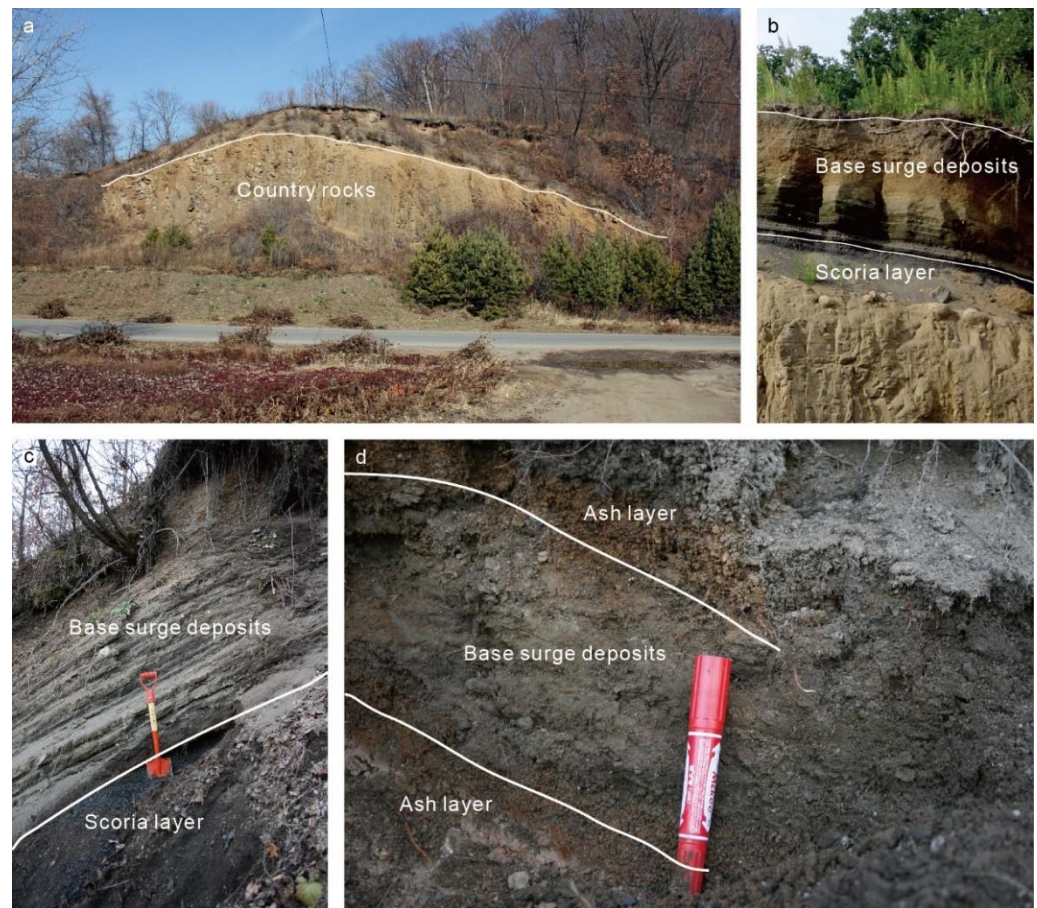


Figure 6. The medial and distal strata of XDDZ: (a) overview of base surge depositing on a small hill; (b) medial base surge and scoria layers at the top of the hill in Lg-94; (c) medial base surge and scoria layers on the foot of the hill in Lg-95; (d) distal base surge and ash layers on the opposite side of the hill in Lg-96.

Lg-95 ($42^{\circ}21'28.40''$ N, $126^{\circ}22'24.27''$ E) is located at the foot of the hill in the northeast of XDDZ, 430 m away from the center of the XDDZ northern crater (Figure 6c). It has a similar stratigraphic sequence to Lg-11 and Lg-94, which has 3 layers. It has a maximum thickness of 4 m. At the bottom of Lg-95, layer 1 is a 1 m scoria layer. In the middle, layer 2 is 2.7 m base-surge deposits, with lithic breccia and cross bedding, along the slope inclination. In the top, layer 3 is a 30 cm black scoria-fall deposit with many plant roots.

4.2.4. Distal Stratigraphic Characteristics from the Northern Crater

Lg-96 ($42^{\circ}21'37.03''$ N, $126^{\circ}21'53.40''$ E) is located on the opposite side of the hill in the north of XDDZ, 770 m away from the center of the XDDZ northern crater (Figure 6d). It has three layers. At the bottom, layer 1 is a 4 cm yellow ash layer. In the middle, layer 2 is a 12 cm grey base-surge deposit, supported by an ash matrix. At the top is a 3 cm yellow ash layer.

4.2.5. Stratigraphic Correlation

In this work, we correlate Lg-75, Lg-77, Lg-11, Lg-94, Lg-95, and Lg-96 using a combination of stratigraphic data (Figure 7). These sections were chosen because they are distributed from proximal to distal facies, and most of them are well-exposed.

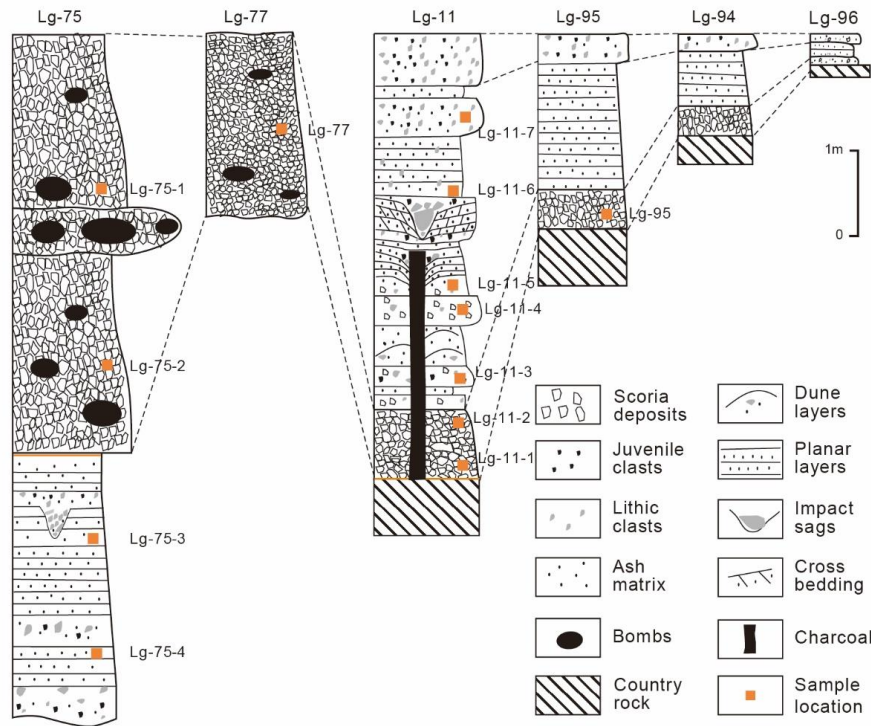


Figure 7. Stratigraphic columns in XDDZ maar.

Ballistic bombs are observed in the scoria deposits of Lg-75, Lg-77, and Lg-11. These scoria deposits are poorly sorted. All of them reflect tephra ring features. Proximal impact sags were deposited in Lg-11 and Lg-75. A vertical facies change occurs from dune beds, cross beds, planar beds, explosive breccia beds, and ash beds. In Lg-94 and Lg-95 of the medial strata, base-surge climbed over the north hill up to a height of 30 m, with planar beds. The distal facies in Lg-96 show that the base-surge deposits mainly consist of two scoria-fall layers and an ash-supported layer, which is probably ash cloud deposits.

The stratigraphic sequence in the XDDZ volcano comprises base-surge deposits and scoria fall deposits from the southern crater and base-surge deposits and scoria fall from the northern crater. The eruptive scale of southern crater was stronger than the scale of northern crater.

4.3. ¹⁴C Dating Result

The ¹⁴C dating data for the carbonized tree in the Lg-11 profile is presented in Table 2 with the previous results. The age is 15,900 ± 70 a BP, which is consistent with the results of previous ages.

Table 2. Radiocarbon ages.

Sample No.	Lab No.	Sample Site	Material	Age (aBP)	Calibrated Age (Cal a BP)	References
1	CG-5721	the scoria layer	Charred Material	15,965 ± 145	19,291 to 18,999	Bai et al., 2006 [5]
Lg-12	422461	Base-surge layer	Charred Material	15,590 ± 50	18,920 to 18,755	Zhao et al., 2021 [15]
Lg-11	441078	Base-surge and scoria layers	Charred Material	15,900 ± 70	19,375 to 18,980	This study

Sample 1 was tested in the ¹⁴C Lab of the Institute of Geology, China Earthquake Administration. Samples Lg-11 and Lg-12 were tested in the Beta Lab.

4.4. Grain Size Distribution

Grain size distribution is an important feature of pyroclastic rock, as it records information about the mechanisms of pyroclastic formation and transportation. According to the stratigraphic characteristics of XDDZ, we divided the XDDZ samples into base-surge and scoria fall. Utilizing these parameters of granulometry, a σ_ϕ - Md_ϕ diagram was plotted.

The σ_ϕ values of the base-surge samples range from 1 to 3, whereas their Md_ϕ values range from -3 to 1 , and their α_ϕ values range from -0.3 to 0.6 (Figure 8b).

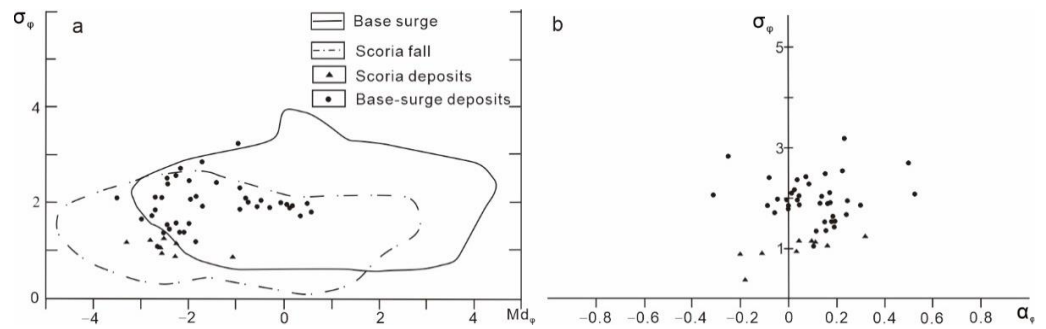


Figure 8. (a) Diagram of median diameter (Md_ϕ) versus sorting (σ_ϕ) (Walker, 1983); (b) diagram of sorting (σ_ϕ) versus skewness (α_ϕ).

The σ_ϕ values of the scoria samples in the southern crater range from 0.89 to 1.24. The Md_ϕ values range from -2.6 to -3.3 . The α_ϕ values of scoria fall range from 0.02 to 0.4 (Figure 8b). The σ_ϕ values of scoria samples in the northern crater range from 0.83 to 0.87, whereas their Md_ϕ values range from -1.05 to -2.55 , and their α_ϕ values range from -0.2 to -0.105 .

The grain-size histograms of scoria fall are single-peak (Figure 9). Most of the base-surge deposits have multiple peaks (Figure 9).

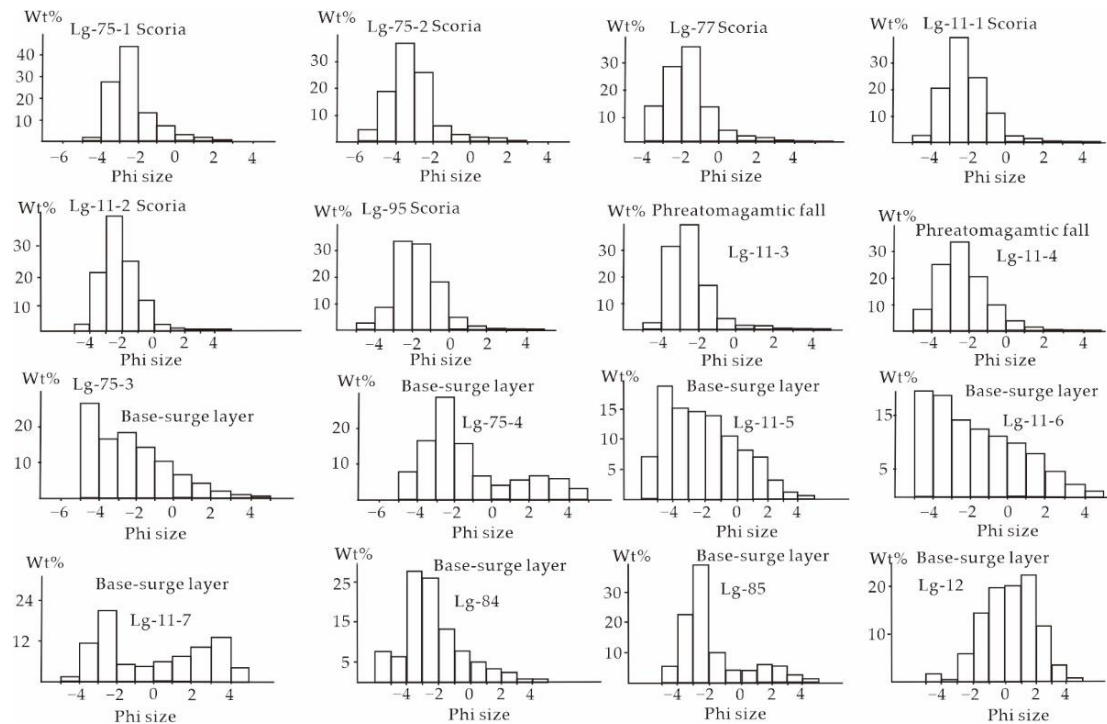


Figure 9. Typical grain-size histograms in the scoria and base surge layers.

4.5. SEM Analysis

SEM analysis is widely used in volcanic studies, especially to analyze surface features and microstructure [12].

In the thin section, samples from the base-surge deposits of Lg-11 record stratification features with micro sag-like structures (Figure 10a). Most particles are highly compacted volcanic ash particles (Figure 10b).

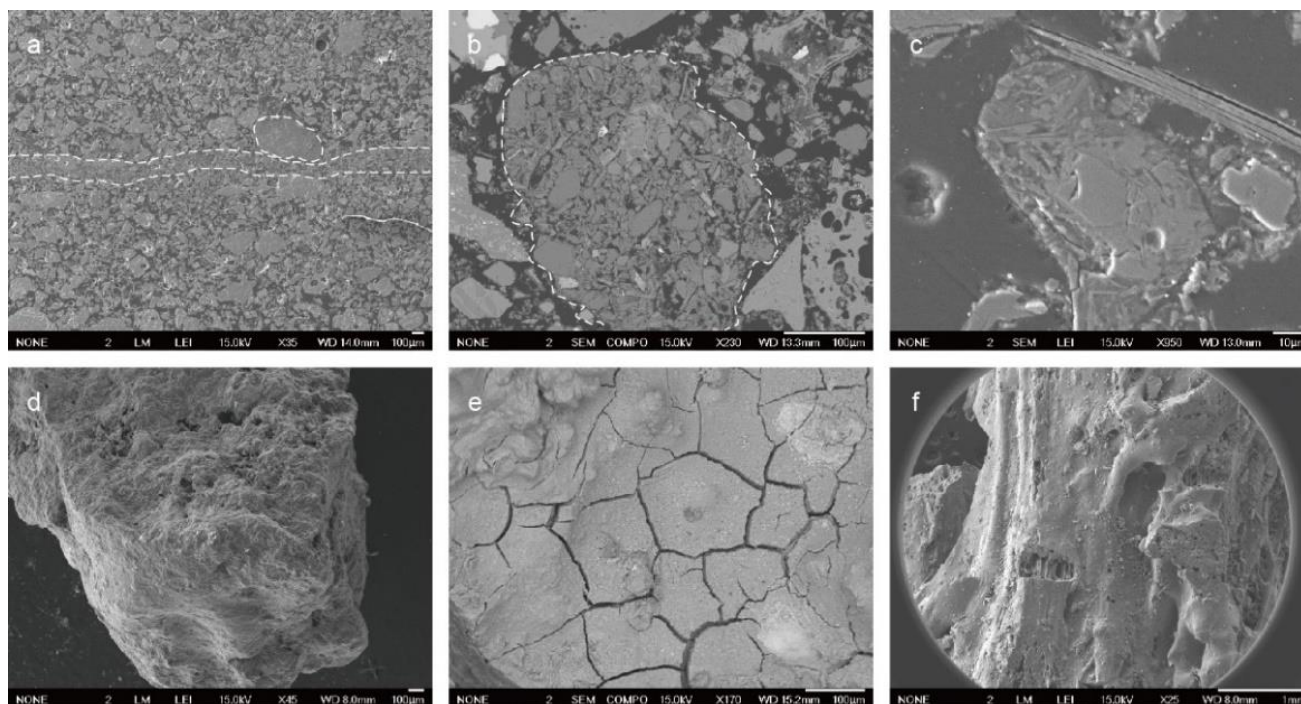


Figure 10. (a) Stratification with micro sag-like structure in the thin section; (b,c) aggregated particles; (d) rough surface of scoria from base-surge deposits; (e) crack surface of scoria close to the carbonized tree; (f) smooth surface of black scoria-fall.

The pyroclasts from the base-surge have the feature of a rough surface with a few vesicles (Figure 10d). The yellow scoria close to the carbonized tree have a surface with quench cracks, adhering particles, and circular bulges (Figure 10e). The black scoria surface is smooth with regular vesicles (Figure 10f).

4.6. Major Elements Analysis

In this paper, we use the total alkali-silica (TAS) diagram to classify the geochemical features of XDDZ. The components of the samples at the profiles of Lg-11 and Lg-75 are in the trachybasalt zone (Table 3 and Figure 11). Fan et al., 1999 also proposed that the Jinlongdingzi volcanic rock is trachybasalt [58]. The XDDZ samples have the same TAS characteristics with Jinlongdingzi rocks.

Table 3. Results of major elements in XDDZ.

NO.	SiO ₂	Al ₂ O ₃	TiO ₂	Fe ₂ O ₃	FeO	CaO	MgO	K ₂ O	Na ₂ O	MnO	P ₂ O ₅	LOI	Total
Lg-11	49.29	15.45	2.12	2.56	8.12	7.26	8.09	1.97	3.65	0.17	0.54	0.51	99.73
Lg-75	48.67	16.79	2.21	4.84	6.37	6.47	6.52	1.85	3.24	0.17	0.58	2.03	99.74

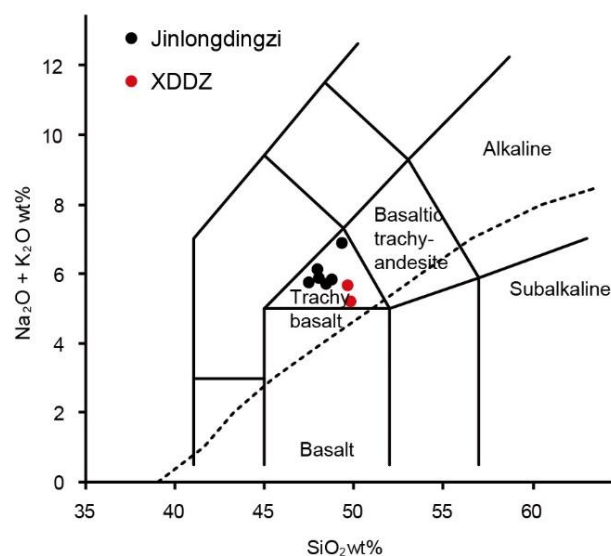


Figure 11. TAS classification diagram of volcanic rocks in the XDDZ maar and Jinlongdingzi volcano (subalkaline–alkaline discrimination line from Rickwood, 1989 [58]; the Jinlongdingzi data are from Fan et al., 1999 [59]).

5. Discussion

The ^{14}C age and stratigraphic evidence show that XDDZ is the youngest maar volcano in the LVF (Tables 2 and 4). However, the destruction of the XDDZ tephra ring is the most serious among these maars. There are two main reasons. First, parts of lava flows from Jinlongdingzi and Beishan volcano destroyed the southern tephra ring of XDDZ. The emplacement of the lava flow from Jinlongdingzi also raised the terrain in the east of the valley and made the area of XDDZ maar a low terrain, especially inside the crater. Therefore, as the water from the hills passed through XDDZ, the inside of the craters gradually became a swamp. Second, agriculture also played an important role. The local peasants reformed part of the swamp in the craters to grow rice and dug the northern tephra ring to collect the pyroclasts for building roads and houses. Fortunately, the local government has protected the rest of the swamps and the volcanic landforms. The Beishan lava flow participated in the destruction of the southern tephra ring. This indicates that the formation age of the Beishan lava flow is younger than the XDDZ formation age. The ^{14}C age show that the Jinlongdingzi lava was formed between 1965 ± 30 a. BP and 2285 ± 60 a. BP [19]. According to the contact relationship between the two lava flows and the tephra ring in the field, it is possible that the Beishan lava was one of the Holocene effusive eruptions in the Jinchuan valley. There were another two Holocene eruptive events in the Jinchuan Valley, and one eruptive event at $14,430 \pm 40$ a. BP near the Jinchuan valley [15]. Therefore, for the last 20,000 years, the Jinchuan valley has been the most active area in the LVF.

Table 4. Ages of some maars in the LVF.

Sample NO.	Location	Age of K-Ar	References
PH139-2	Sihailongwan	0.05 ± 0.1 Ma, 0.21 ± 0.2 Ma	Fan et al., 2002 [18]
Lg9931	Donglongwan	0.08 ± 0.1 Ma, 0.14 ± 0.1 Ma	Fan et al., 2002 [18]
Lg98021-2b	Dalongwan	0.55 ± 0.22 Ma	Fan et al., 2002 [18]
PH143-1	Longquanlongwan	0.60 ± 0.03 Ma	Fan et al., 2002 [18]

There are at least 13 volcanoes within 5 km of XDDZ. The source volcano of the strata in Lg-11 is disputed. Bai et al., 2006 proposed that the strata near Lg-11 were from Dawengquan maar [5], which was 1.4 km away from Lg-11, separated by a hill. Due to the excavation of local people, more stratigraphic sections have been found. The volcanic bombs and sag structure in Lg-11 prove that these sections are the volcanic productions of crater facies, not distal volcanic productions. There is no interruption between base-surge and scoria-fall layers. The carbonized tree is also good evidence to show that the base-surge and scoria-fall layers were formed in the same eruptive event. The continuous sections from Lg-75 to Lg-11 show that the scoria layer in Lg-11 is from the southern crater and that the scoria stratum under Jinchuan town is also from the XDDZ. Both the base-surge deposits and the scoria near Lg-11 were formed in the XDDZ eruptive event.

The stratigraphic evidence shows that the hill has partly affected the transportation and deposition of the XDDZ base-surge. On the windward slope, the base-surge of Lg-95 deposited 2.7 m strata at the foot because of gravity. At the top of the hill, the thickness of Lg-94 changed to 1.3 m, only 90 m away from Lg-95. After climbing over the hill with a height of 30 m, 700 m away from the center of the northern crater, it turned to ash cloud deposits. The ash cloud, belonging to a part of the base-surge, with suspended transportation, can move independently [60]. The main flow unit of the base-surge was limited by the hills. However, the ash cloud could have escaped the hill topography and floated further.

Most of base-surge deposits are very poorly sorted, and their histograms have multi-peak features. The grain-size of scoria fall decreases from the southern crater to the northern crater. Most of scoria samples in the southern crater are poorly sorted. However, scoria fall samples from the northern crater are moderately sorted. According to the geological work, the scoria fall in the southern crater is in the crater lithofacie area, involved with some ballistic production. The scoria fall in the northern crater is from the southern crater, experiencing 700 m transportation. Therefore, they have a smaller size and are moderately sorted.

Temperature is one of important physical parameters of the base-surge. According to the results of direct measurements of volcano eruption in recent decades, Lerner et al., 2021 summarized that temperature in low energy surges was to be at least 180 °C to over 410 °C [61]. However, for many unrecorded or prehistoric phreatomagmatic eruptions, it is hard to estimate the accurate temperature. The strata of base-surges carry some temperature information about the physical processes. Wohletz, 1998 lists the stratigraphic characteristics of the cool wet surges and hot dry surges [62]. Massive beds and poorly developed bedding show that the base-surge is probably cool and wet. The base-surge deposits in Lg-75 of the southern crater have the same features. The abundant dune structure and well-developed thin bedding indicate that the base-surge is hot and dry. The strata of Lg-11 in the northern crater agree with these characteristics. The carbonized wood in the northern tephra ring provides a clue to estimate the base-surge temperature in the northern crater. Pensa et al., 2019 chose 28 standing carbonized trees in situ, formed in the July 2015 eruption of Colima [63]. The formation temperatures of these carbonized trees in the proximal valley were between 357 °C and 371 °C. The carbonized trees of XDDZ, located in the northern tephra ring, are closer to the crater. This indicates that the carbonized trees of XDDZ had a higher formation temperature. The temperature was probably over 371 °C.

The sequence shows that the eruptions in XDDZ maar started with a phreatomagmatic eruption, then turned to a magmatic eruption and a phreatomagmatic eruption, and then ended with a smaller magmatic eruption. It is very rare that magmatic eruptions are active between two phreatomagmatic eruptions [2]. In hard-rock valleys, faults are more hydraulically active [1,2]. The exposed country rocks show that it is a hard substrate area in the LVF. The fissure system effect should be taken into consideration. Liu, 1999 presented that there were three fissure systems in the LVF, including a NE-trending fault, a NW-trending fault, and a WE-trending fault [53]. The trend of Jinchuan valley consists of two directions:

NE-trending in the southeast and WE-trending in the east. The volcanoes in the Jinchuan valley mainly occur in the directions of NE-trending and WE-trending. The topographic results show that a low-velocity layer exists in the middle crust under the Jinlongdingzi volcano along the WE direction. This phenomenon indicates that the distribution of thermal activity is probably related to the tectonic distribution. The migration of eruptive vents from the southwest to northeast in XDDZ indicates that the NE-trending fissure system affected the eruptive processes.

Due to the serious destruction, it is hard to get the original depth of XDDZ craters. Ross et al., 2011 estimated that the youngest maar craters had diameter/depth ratios between 3 and 7 in the hard rock area [11]. According to his estimation and the diameters of XDDZ, it is inferred that the crater depth of the southern crater had a range of 200 to 467 m, and that the northern crater had a range of 43 to 100 m. The eruptive depth is also an important parameter to understand phreatomagmatic behavior. Based on the study of different models, Taddeucci et al., 2010, proposed that shallow explosions possibly accounted for a large fraction of the total energy release in maar formation [64]. Phreatomagmatic eruptions are likely sourced mostly by explosions in the uppermost ~200 m [65]. Valentine et al., 2014 proposed that repeated explosions, further brecciation, and subsidence led to the development of a mature maar system [65]. It also indicates that the explosion depth is probably deeper than the crater depth. Above all, the water in the fissure system participating in the eruption was probably in the depth range from 43 to 200 m in XDDZ.

The change from phreatomagmatic eruption to magmatic eruption is often considered to be the result of water running out [1]. In XDDZ maar, the eruptive changes were complex, from a phreatomagmatic eruption to a magmatic eruption, and then to a phreatomagmatic eruption, and finally to a magmatic eruption. It is hard to use water depletion to explain these changes in the hard rock area. Valentine et al., 2017 proposed that increasing magma flux probably overwhelmed the effects of water [17]. The cauliflower and bread-crust bombs in the bomb-rich layer of Lg-75 indicate that these ballistic bombs were probably affected by water. Additionally, the large amount of scoria fall was hardly affected by water, because the scoria surface is smooth, without any quenching structure. After these eruptions, the smaller phreatomagmatic eruption occurred again in the XDDZ area. This phenomenon agrees with the recent evolutionary model [17].

It was inferred that a thermal conduction of magma existed in lower crust under the Jinlongdingzi volcano [51]. The magma rose along the fissure system under the Jinchuan valley (Figure 12). Up to ~200 m from the surface, the magma activity interacted with water in the fissure. The first phreatomagmatic eruption occurred. After that, it turned into a magma explosive eruption. The rising channel was blocked because of previous eruptions. The small scale of magma along the NE-trending fissure was up to 43~200 m and interacted with the fissure water. It took place during the second phreatomagmatic eruption. At last, it all ended with a small explosive eruption.

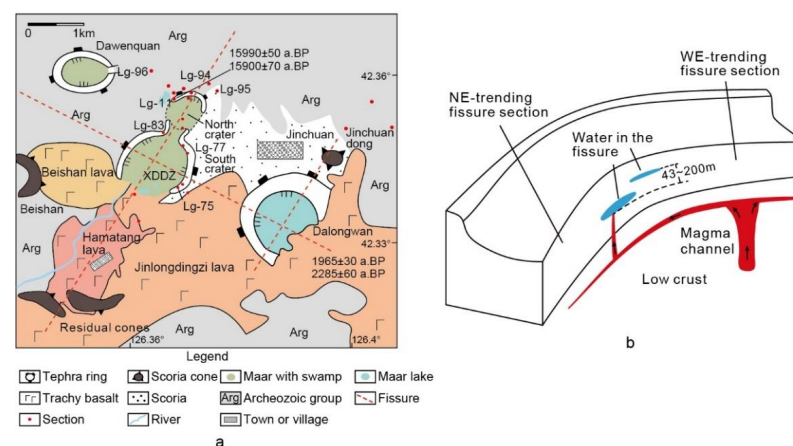


Figure 12. Cont.

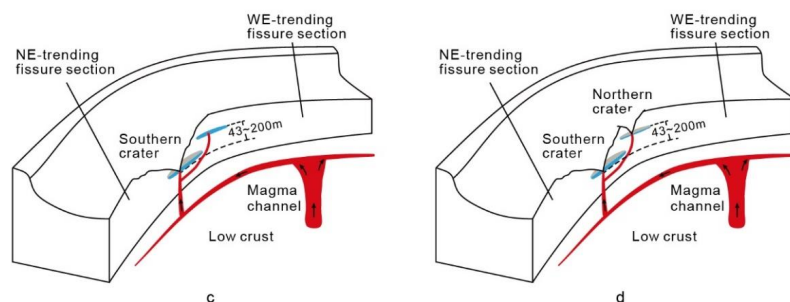


Figure 12. (a) Geology map of XDDZ area; (b–d) the formation model of XDDZ in the Jinchuan valley (not in scale).

6. Conclusions

The XDDZ maar was formed in the late Pleistocene, experiencing two cycles from phreatomagmatic eruption to explosive magmatic eruption. These eruptions produced two craters with complex stratigraphic sequences. The migration of the eruptive vents in XDDZ from south to north was controlled by the NE-trending fissure in the hard rock area (Figure 12). The stratigraphic evidence shows that water was not the only factor controlling the alternation between the phreatomagmatic eruptions and the magmatic eruptions in XDDZ. The magma flux probably played an important role in the changes of eruptive style. Longwans with complicated eruptive sequence and several craters probably have the same formation model as XDDZ in the LVF.

The XDDZ base-surge climbed over a small hill and ran out a distance of less than 1 km with a high emplacement temperature. The accompanied ash cloud and fallout scoria were able to escape the local topography. All of above provide insights on the base-surge destruction in the LVF. In order to prevent potential base-surge hazard, the local government should reduce the construction and living in the valley.

Author Contributions: Conceptualization, B.Z. and D.X.; methodology, B.Z. and Z.B.; software, Z.C. and B.Z.; validation, B.Z., D.X. and Z.B.; formal analysis, B.Z.; investigation, B.Z. and Z.C.; resources, B.Z.; data curation, B.Z.; writing—original draft preparation, B.Z.; writing—review and editing, B.Z.; visualization, B.Z.; supervision, B.Z.; project administration, B.Z.; funding acquisition, B.Z. All authors have read and agreed to the published version of the manuscript.

Funding: This work was supported by the National Science Foundation Project (Grant No. 41402299) and the Fundamental Scientific Research Project of the Institute of Geology, China Earthquake Administration (IGCEA1516 and IGCEA1903).

Data Availability Statement: The data supporting the conclusion of this paper will be made available by the authors, without undue reservation, to any qualified researcher.

Acknowledgments: We are grateful to all the reviewers for their valuable advice. We express deep gratitude to Jing Pu, Tao Zhang, Jialong Wang, Jianli Sui and all the staff of LVF Observation Station for their assistance in the field work, and Xiaomin Liao for the help of drawing.

Conflicts of Interest: The authors declare no conflict of interest.

References

1. Lorenz, V. On the formation of maars. *Bull. Volcanol.* **1973**, *37*, 183–204. [[CrossRef](#)]
2. Lorenz, V. Maar-diatreme volcanoes, their formation, and their setting in hard-rock or soft-rock environments. *Geolines* **2003**, *15*, 72–83.
3. Németh, K. Monogenetic volcanic fields: Origin, sedimentary record, and relationship with polygenetic volcanism. *Geol. Soc. Am. Spec. Pap.* **2010**, *470*, 43–66.
4. Ngwa, C.; Suh, C.; Devey, C.W. Phreatomagmatic deposits and stratigraphic reconstruction at Debunscha Maar (Mt Cameroon volcano). *J. Volcanol. Geotherm. Res.* **2010**, *192*, 201–211. [[CrossRef](#)]
5. Bai, D.; Xu, B.; Zhang, L.; Zhang, T.; Bu, J. Study on type and phase of Quaternary explosive volcanism in Longgang volcanic cluster. *Acta Petrol. Sin.* **2006**, *22*, 1473–1480. (In Chinese with English Abstract).

6. Freda, C.; Gaeta, M.; Karner, D.B.; Marra, F.; Renne, P.R.; Taddeucci, J.; Scarlato, P.; Christensen, J.N.; Dallai, L. Eruptive history and petrologic evolution of the Albano multiple maar (Alban Hills, Central Italy). *Bull. Volcanol.* **2006**, *68*, 567–591. [\[CrossRef\]](#)
7. Houghton, B.; Schmincke, H.-U. Mixed deposits of simultaneous strombolian and phreatomagmatic volcanism: Rothenberg volcano, east Eifel volcanic field. *J. Volcanol. Geotherm. Res.* **1986**, *30*, 117–130. [\[CrossRef\]](#)
8. Houghton, B.; Wilson, C.; Smith, I. Shallow-seated controls on styles of explosive basaltic volcanism: A case study from New Zealand. *J. Volcanol. Geotherm. Res.* **1999**, *91*, 97–120. [\[CrossRef\]](#)
9. Lorenz, V.; Zimanowski, B. Volcanology of the West Eifel Maars and its relevance to the understanding of kimberlite pipes. In Proceedings of the 9th International Kimberlite Conference Field Trip, Frankfurt, Germany, 7–10 & 16–18 August 2008; pp. 7–10.
10. Ort, M.H.; Carrasco-Núñez, G. Lateral vent migration during phreatomagmatic and magmatic eruptions at Tecuitlapa Maar, east-central Mexico. *J. Volcanol. Geotherm. Res.* **2009**, *181*, 67–77. [\[CrossRef\]](#)
11. Ross, P.S.; Delpit, S.; Haller, M.J.; Németh, K.; Corbaella, H. Influence of the substrate on maar–diatreme volcanoes—An example of a mixed setting from the Pali Aike volcanic field, Argentina. *J. Volcanol. Geotherm. Res.* **2011**, *201*, 18. [\[CrossRef\]](#)
12. Tchamabé, B.C.; Kereszturi, G.; Németh, K.; Carrasco-Núñez, G. How Polygenetic are Monogenetic Volcanoes: Case Studies of Some Complex Maar-Diatreme Volcanoes. In *The Updates in Volcanology-From Volcano Modelling to Volcano Geology*; Németh, K., Ed.; InTech: Vienna, Austria, 2016; Chapter 13.
13. Tchamabé, B.C.; Ohba, T.; Kereszturi, G.; Németh, K.; Aka, F.T.; Youmen, D.; Miyabuchi, Y.; Ooki, S.; Tanyileke, G.; Hell, J.V. Towards the reconstruction of the shallow plumbing system of the Barombi Mbo Maar (Cameroon) Implications for diatreme growth processes of a polygenetic maar volcano. *J. Volcanol. Geotherm. Res.* **2015**, *301*, 293–313. [\[CrossRef\]](#)
14. White, J.D.; Ross, P.S. Maar-diatreme volcanoes: A review. *J. Volcanol. Geotherm. Res.* **2011**, *201*, 1–29. [\[CrossRef\]](#)
15. Zhao, B.; Xu, D.B.; Bai, Z.D.; Chen, Z.Q. Volcanism in the Longgang volcanic field of NE China: Insights from eruption history, volcano types and geochemical characteristics. In *The Active volcanoes of China*; Xu, J., Oppenheimer, C., Hammond, J., Wei, H., Eds.; Geology of London Society, Special Publication: Bath, UK, 2021; p. 510.
16. Zhao, B.; Xu, J.D.; Pan, B.; Yu, H.M. Preliminary study on grain size distribution and transportation characteristics of the base-surge deposits near Longquanlongwan volcano crater in Jilin. *Acta Petrol. Sin.* **2008**, *24*, 2631–2637. (In Chinese with English Abstract).
17. Valentine, G.A.; White, J.D.L.; Ross, P.S.; Graettinger, A.H.; Sonder, I. Updates to Concepts on Phreatomagmatic Maar-Diatremes and Their Pyroclastic Deposits. *Front. Earth Sci.* **2017**, *5*, 68. [\[CrossRef\]](#)
18. Fan, Q.C.; Sui, J.L.; Liu, R.X.; Wei, H.Q.; Li, D.M.; Sun, Q.; Li, N. Period of Quaternary volcanic activity in Longgang area, Jilin Province. *Acta Petrol. Sin.* **2002**, *18*, 495–500. (In Chinese with English Abstract).
19. Liu, J.Q.; Chu, G.Q.; Han, J.T.; Rioual, P.; Jiao, W.Y.; Wang, K.J. Volcanic eruptions in the Longgang volcanic field, northeastern China, during the past 15000 years. *J. Asian Earth Sci.* **2009**, *34*, 645–654. [\[CrossRef\]](#)
20. Liu, J.Q.; Negendank, J.F.W.; Wang, W.Y.; Chu, G.Q.; Mingram, J.; Guo, Z.F.; Luo, X.J.; Chen, R.; Liu, D.S. The distribution and geological characteristics of maar lakes in China. *Quat. Sci.* **2000**, *20*, 78–86. (In Chinese with English Abstract).
21. Liu, Q.; Wei, H.Q.; Xu, J.D.; Luan, P.; Sun, C.Q.; Pan, B.; Zhao, B.; Yu, H.M. Grain size characteristics of the tephra sheet and their geological implication. *Seismol. Geol.* **2009**, *31*, 112–121. (In Chinese with English Abstract).
22. Liu, R.X. Jinlongdingzi volcano in the Longgang volcanic field. In *Active Volcanoes in China*; Liu, R.X., Ed.; Seismological Press: Beijing, China, 2000; pp. 67–74. (In Chinese)
23. Liu, X.; Xiang, T.Y. Study on fallout tephra deposits in Dayizishan. *J. Chang. Univ. Earth Sci.* **1991**, *21*, 417–424. (In Chinese with English Abstract).
24. Liu, X.; Zhang, C.L. Sihai basaltic scoria deposits in the Longgang volcanic swarm belong to the sub-plinian eruption of Jinglongdingzi volcano. *Jilin Geol.* **1997**, *3*, 1–8. (In Chinese with English Abstract).
25. Luo, Z.H. The study of ultramafic nodules in Dayizishan basalt, Huinan County, Jilin Province. *Earth Sci. J. Wuhan Coll. Geol.* **1984**, *24*, 81–86. (In Chinese with English Abstract).
26. Shi, L.B.; Lin, C.Y.; Han, X.L.; Chen, X.D. Principal features of mantle xenoliths in Jinlongdingzi volcano, Longgang volcano cluster, Jilin Province and their geological implications. *Geol. Rev.* **1999**, *45*, 308–318. (In Chinese)
27. Sui, J.L.; Fan, Q.C.; Cao, J. A preliminary study of eruption features and petro-chemistry of volcanic rocks from the Longgang volcanoes. *Geol. Rev.* **1999**, *45*, 319–324. (In Chinese)
28. Wang, Y.J.; Sun, J.Z. Preliminary Division of the Cenozoic Longgang volcano cluster, Jilin Province. *Jilin Geol.* **1980**, *3*, 6–25. (In Chinese with English Abstract).
29. Wang, Y.S.; Jin, K. Division and eruption types of the Cenozoic Longgang volcano cluster, Jilin Province. *Geol. Rev.* **1999**, *45*, 332–337. (In Chinese)
30. Wei, H.Q.; Liu, R.X.; Fan, Q.C.; Jin, B.L.; Liu, X.; Zhang, C.L. Monogenetic volcanism in Longgang volcano clusters. *Geol. Rev.* **1999**, *45*, 325–331. (In Chinese)
31. Xu, D.B.; Bai, Z.D.; Zhang, B.L.; Hong, H.J. Characteristic and genetic mechanism of pyroclastic base-surge deposits of volcanic swarm in Longgang area, Jilin province. *Acta Sedimentol. Sin.* **2005**, *23*, 60–66. (In Chinese with English Abstract).
32. Yan, J.; Zhao, X.J.; Liu, H.Q. Quaternary basalts from Longgang in the North China Craton: Petrogenesis and characteristics of the mantle source. *Acta Petrol. Sin.* **2007**, *23*, 1413–1422. (In Chinese with English Abstract).
33. Yang, Q.F.; Wang, J.; Hattori, K.H.; Pan, X.D.; Liu, J.L.; Xie, Z.P.; Song, Y. Redox state of the lithospheric mantle beneath Huinan-Jingyu area, southern Jilin Province, China. *Acta Petrol. Sin.* **2011**, *27*, 1797–1809. (In Chinese with English Abstract).

34. Yu, H.M.; Xu, J.D.; Lin, C.Y.; Zhao, B. Study on the characteristics of Quaternary volcanic products from Nanlongwan volcano, Longgang volcanic cluster, Jilin Province. *Acta Petrol. Sin.* **2008**, *24*, 2621–2630. (In Chinese with English Abstract).
35. Yu, H.M.; Xu, J.D.; Wu, J.P.; Luan, P.; Zhao, B. Numerical simulation and probabilistic hazard assessment of tephra fallout at Jinlongdingzi volcano, Longgang volcanic field in Jilin Province. *Technol. Earthq. Disaster Prev.* **2013**, *8*, 62–70. (In Chinese)
36. Xu, Y.G.; Huang, X.L.; Thirlwall, M.F.; Chen, X.M. Reactive harzburgite xenoliths from Huinan, Jilin province and the implications for deep dynamic processes. *Acta Petrol. Sin.* **2003**, *19*, 18–26. (In Chinese with English Abstract).
37. Yu, F.S.; Yuan, W.M.; Han, S.; Ma, Z.B.; Jin, K. U-Series component dating for late Pleistocene basalt of Longgang, Jinlin province. *High Energy Phys. Nucl. Phys.* **2003**, *27*, 1039–1044. (In Chinese)
38. Zhao, B.; Xu, J.D.; Yu, H.M. Grain-size characteristics of pyroclasts in Changbaish mountain area. *Seismol. Geol.* **2010**, *32*, 233–242. (In Chinese with English Abstract).
39. Zhao, B.; Zhang, T.; Xu, D.B.; Bai, Z.D. Preliminary volcanic hazard zonation in Jinlongdingzi volcano, Longgang volcano area, Jilin Province, China. *Seismol. Geol.* **2017**, *39*, 423–432. (In Chinese with English Abstract).
40. Zhang, B.L.; Bai, Z.D.; Hong, H.J.; Xu, D.B.; Pan, X.D. A fractal study on the pyroclasts from the longang volcano, Jilin Province. *Seismol. Geol.* **2005**, *27*, 462–469. (In Chinese with English Abstract).
41. Chu, G.Q.; Liu, J.Q.; Schettler, G.; Li, J.Y.; Sun, Q.; Gu, Z.Y.; Lu, H.Y.; Liu, Q.; Liu, T.S. Sediment fluxes and varve formation in Sihailongwan, a maar lake from northeastern China. *J. Paleolimnol.* **2005**, *34*, 311–324.
42. Chu, G.Q.; Sun, Q.; Rioual, P.; Boltovskoy, A.; Liu, Q.; Sun, P.Q.; Han, J.T.; Liu, J.Q. Dinocyst microlaminations and freshwater “red tides” recorded in Lake Xiaolongwan, northeastern China. *J. Paleolimnol.* **2008**, *39*, 319–333. [[CrossRef](#)]
43. Chu, G.Q.; Sun, Q.; Gu, Z.Y.; Rioual, P.; Liu, Q.; Kaijun, W.; Han, J.T.; Liu, J.Q. Dust records from varved lacustrine sediments of two neighboring lakes in northeastern China over the last 1400 years. *Quat. Int.* **2009**, *194*, 108–118.
44. Frank, U. Rock magnetic studies on sediments from Erlongwan maar lake, Long Gang Volcanic Field, Jilin province, NE China. *Geophys. J. Int.* **2007**, *168*, 13–26. [[CrossRef](#)]
45. Guo, Z.F.; Liu, J.Q.; Fan, Q.C.; He, H.Y.; Sui, S.Z.; Chu, G.Q.; Liu, Q.; Negendank, J. Source of volcanic ash in the sediments of Sihailongwan maar lake, NE China, and its significance. *Acta Petrol. Sin.* **2005**, *21*, 251–255.
46. Mingram, J.; Allen, J.R.; Brüchmann, C.; Liu, J.Q.; Luo, X.; Negendank, J.; Nowaczyk, N.; Schettler, G. Maar-and crater lakes of the Long Gang Volcanic Field (NE China)—overview, laminated sediments, and vegetation history of the last 900 years. *Quat. Int.* **2004**, *123*, 135–147. [[CrossRef](#)]
47. Schettler, G.; Liu, Q.; Mingram, J.; Stebich, M.; Dulski, P. East-Asian monsoon variability between 15 000 and 2000 cal. yr BP recorded in varved sediments of Lake Sihailongwan (northeastern China, Long Gang volcanic field). *Holocene* **2006**, *16*, 1043–1057. [[CrossRef](#)]
48. Liu, X.; Xiang, T.Y.; Wang, X.K. Episondes of Cenozoic volcanism in the Changbai Mountains area. *Jilin Geol.* **1989**, *1*, 30–41. (In Chinese with English Abstract).
49. Liu, J.Q.; Ding, G.; Zhang, C.X.; Wu, C.Z. Study on present activity of Longgang volcano in Jilin Province. *North China Earthq. Sci.* **2013**, *31*, 112–121. (In Chinese with English Abstract).
50. Qi, W.; Liu, J.Q.; Li, Z.W.; Liu, D.F.; Jin, W. Preliminary discussion on the risk of volcano eruption in Longgang area. *J. Disaster Prev. Reduct.* **2013**, *29*, 70–73. (In Chinese)
51. Pang, G.H.; Feng, J.K.; Lin, J. Crust structure beneath Jilin Province and Liaoning Province in China: Based on seismic ambient noise tomography. *J. Volcanol. Geotherm. Res.* **2016**, *327*, 249–256. [[CrossRef](#)]
52. Liu, J.Q. *Volcanoes in China*; Science Press: Beijing, China, 1999; pp. 122–124.
53. Liu, X. Tectonic control of Cenozoic volcanism in Northeastern China. *World Geol.* **1999**, *2*, 23–29.
54. Wei, W.; Xu, J.; Zhao, D.; Shi, Y. East Asia mantle tomography: New insight into plate subduction and intraplate volcanism. *J. Asian Earth Sci.* **2012**, *60*, 88–103. [[CrossRef](#)]
55. Zhao, D.; Liu, L. Deep structure and origin of active volcanoes in China. *Geosci. Front.* **2010**, *1*, 31–44. [[CrossRef](#)]
56. BGMSJ. *Bureau of Geology and Mineral Resources of Jilin Province*; Geology Investigation Report of Jingyu County; Geological Publishing House: Beijing, China, 1979; pp. 270–272. (In Chinese)
57. Inman, D.L. Measures for describing the size distribution of sediments. *J. Sediment. Res.* **1952**, *22*, 125–145.
58. Rickwood, P.C. Boundary lines within petrologic diagrams which use oxides of major and minor elements. *Lithos* **1989**, *22*, 247–263. [[CrossRef](#)]
59. Fan, Q.C.; Liu, R.X.; Wei, H.Q.; Sui, J.L.; Li, N. The petrology and geochemistry of Jinlongdingzi modern active volcano in Longgang area. *Acta Petrol. Sin.* **1999**, *15*, 584–589. (In Chinese with English Abstract).
60. Cas, R.A.F.; Wright, J.V. *Volcanic Successions: Modern and Ancient*; Allen and Unwin: London, UK, 1987; pp. 117–119.
61. Lerner, G.A.; Jenkins, S.F.; Charbonnier, S.J.; Domorowski, J.C.; Baxter, P.J. The hazards of unconfined pyroclastic density currents: A new synthesis and classification according to their deposits, dynamics, and thermal and impact characteristics. *J. Volcanol. Geotherm. Res.* **2021**, *421*, 107429. [[CrossRef](#)]
62. Wohletz, K.H. Pyroclastic surges and compressible two-phase flow. In *From Magama to Tephra: Modelling Physical Processes of Explosive Volcanic Eruptions*; Freundt, A., Rosi, M., Eds.; Elsevier Science Publications: Amsterdam, The Netherlands, 1998; pp. 247–312.
63. Pensa, A.; Capra, L.; Giordano, G. Ash clouds temperature estimation. Implication on dilute and concentrated PDCs coupling and topography confinement. *Sci. Rep.* **2019**, *9*, 5657. [[CrossRef](#)]

-
64. Taddeucci, J.; Sottili, G.; Palladino, D.M.; Ventura, G.; Scarlato, P. A note on maar eruption energetics: Current models and their application. *Bull. Volcanol.* **2010**, *72*, 75–83. [[CrossRef](#)]
 65. Valentine, G.A.; Graettinger, A.H.; Sonder, I. Explosion depths for phreatomagmatic eruptions. *Geophys. Res. Lett.* **2014**, *41*, 3045–3051. [[CrossRef](#)]